Heterogeneity of the placenta in health and disease explored through integrated histology, gene expression and modelling

Hannah Ee Juen Yong[1,2]*, Kasia Maksym[3,4]*, Muhammad Ashraf Bin Yusoff[3], Esteban Salazar-Petres[1], Tatiana Nazarenko[3,5], Alexey Zaikin[3,5], Anna L David[3,4,6], Sara L Hillman[3,4]+, Amanda N. Sferruzzi-Perri[1]+

*contributed equally; joint first author

+contributed equally; joint last and corresponding author

[1]Centre for Trophoblast Research,
Department of Physiology, Development and Neuroscience
University of Cambridge
Cambridge UK
CB2 3EG

[2]Singapore Institute for Clinical Sciences,
Agency for Science, Technology and Research,
Singapore

[3] Elizabeth Gareth Anderson Institute for Women's Health,
University College London,
84-86 Chenies Mews, London UK
WC1E 6HU

[4] Fetal Medicine Unit
Elizabeth Gareth Anderson Wing,
University College Hospitals NHS Trust,
25 Grafton Way, London UK
WC1E 6DB

[5] Department of Mathematics,
University College London,
London UK

WC1E 6AE

[6] National Institute for Health Research University College London Hospitals Biomedical Research Centre, 149 Tottenham Court Road, London W1T 7DN

Correspondence:
Amanda Sferruzzi-Perri (ans48@cam.ac.uk)
Sara Hillman (sara.hillman@ucl.ac.uk)

Abstract:

Fetal growth restriction (FGR) is a leading cause of perinatal morbidity and mortality. Altered placental formation and functional capacity are major contributors to FGR pathogenesis. Relating placental structure to function across the placenta in healthy and FGR pregnancies remains largely unexplored but could improve understanding of placental diseases. We investigated integration of these parameters spatially in the term human placenta using predictive modelling. Systematic sampling was able to overcome heterogeneity in placental morphological and molecular features. Defects in villous development, elevated fibrosis, and reduced expression of growth and functional marker genes (IGF2, VEGA, SLC38A1, SLC2A3) were seen in age-matched term FGR versus healthy control placentas. Characteristic histopathological changes with specific accompanying molecular signatures could be integrated through computational modelling to predict if the placenta came from a healthy or FGR pregnancy. Our findings yield new insights into the spatial relationship between placental structure and function and the aetiology of FGR.

Key words: Placenta, FGR, modelling, morphology, growth genes, transport

Introduction:

The human placenta is a highly specialized organ in pregnancy, whereby normal functioning is critical to fetal development and long-term health. By acting as a functional interface between the maternal and fetal circulation, it is responsible for maternal-fetal substrate exchange, protects the fetus from immune rejection by the mother and secretes hormones, which maintain pregnancy and promote healthy fetal growth and development[1,2]. This complex organ is structurally heterogeneous, not only in terms of its broad spatial macroscopic characteristics with multiple cotyledons and vascular supply, but also at the microscopic level of the villous tree and trophoblast. Even in pregnancies that deliver at term without any apparent pathology, novel techniques such as micro-CT are now describing the large degree of heterogeneity of vascular density and branching in the placenta[3]. In addition, computational models have predicted that local heterogeneity in placental vascular structure can have major impacts on the resistance of the feto-placental circulation and placental dysfunction[4]. Investigating the spatial relationships between changes in gene expression and structural differences in the placenta is important, so that we may better elucidate the potential functional effect of placental pathology in obstetric disease.

Fetal growth restriction (FGR) is a major cause of perinatal morbidity and mortality. The risk of *in utero* or neonatal death is especially high amongst growth restricted fetuses and neonates who are commonly born preterm [5]. In some regions of the world, FGR and prematurity account for 80% of neonatal deaths[6]. FGR is diagnosed when a fetus fails to reach their genetically predefined growth potential and is often identified by feto-placental ultrasound features (such as increased umbilical artery resistance to blood flow), and subsequently confirmed through placental histopathology[7]. The gestational age at diagnosis is used to further subdivide FGR into early-onset, detected before 32 weeks of gestation, and late-onset according to international consensus[8]. Neonates born following FGR have an increased risk of developing health problems, both in the immediate postnatal period including low blood sugars and poor temperature regulation and feeding, but also in later adult life in the form of cardiovascular and metabolic disease[9,10]. Management of pregnancies affected by FGR can be challenging, as timing of delivery has to be judged well, to balance the hazards of preterm birth against the risks of irreversible damage secondary to intrauterine hypoxia and nutritional deficiency or even stillbirth[11].

The placenta of FGR pregnancies is characterized by reduced syncytiotrophoblast surface area, increased thickness of the exchange barrier formed by the trophoblast and fetal capillary endothelium and an increase in placental apoptosis[12-15]. Whilst it is recognized that there are key mediators of fetal growth that are influenced by placental function including but not limited to transfer of gases[16], glucose[17,18], lipids[19] and amino acids[18,20], understanding the mechanisms through which placental histological changes might be affecting these pathways remains a challenge. Nuanced, integrated investigations will better delineate the underlying functional mechanisms related to the histological changes observed in the placenta. Experimental animal data has highlighted central roles that certain structural and functional changes play in the placenta to fetal growth outcomes[21-25]. However, data on how structure *and* molecular changes together impact on function and on each other, even in the form of nutrient transporter expression, are scarce or not available for the human placenta[26,27].

Better understanding of how placental structure relates to functional capacity is further optimized through robust placental sampling protocols. Methodological errors arise from differences in sampling and/or tissue processing, which has previously hampered the reproducibility and possible extrapolation of placental studies[28,29]. Systematic uniform random sampling involves random selection of the first sampling site, with subsequent sites dictated by a pre-made sampling interval. This method is recommended to ensure representative and unbiased sampling of the placenta[29,30]. It is a simple method, allowing for even coverage of the placenta and ensures that all sites can only be selected once[29]. In practice, however, systematic uniform random sampling has limitations. Firstly, its lack of bias may be compromised if the pre-determined sampling interval coincides with a natural pattern existent in the placenta[30]. Secondly, placentae templates designed for systematic uniform random sampling assume all placentas to be roughly circular in shape, with central umbilical cord insertion. This assumption of a uniform shape and cord insertion however is incorrect. Although studies do show that mean placental chorionic shape at term is round, deviations in placental shape are associated with reduced placental efficiency[31]. In addition, the site of umbilical cord insertion appears to be related to placental function, with a marginal cord insertion near the outer boundary of the placenta being associated with a more asymmetric chorionic vessel structure[32], which has been associated with FGR, stillbirth and neonatal death[33].

While analysis of single sites may miss important histopathological and functional changes, multiple site collection poses analytical challenges, and methods may still fail to identify

critical differences within placentas affected by pathology, such as FGR. Statistical modelling allows for the exploration and integration of multiple data points from the same sample to provide more accurate interpretation of functional consequences. Moreover, the use of modelling to predict regional and disease state differences has high translational potential, for example providing an explanation for why the pregnancy was compromised and which baby may benefit the most from early health monitoring and/or postnatal intervention. With this study we therefore, firstly sought to better understand if systematic uniform random sampling methods could be optimised to the challenges that FGR placentas pose. Secondly, we sought to characterise the degree of detailed histological and molecular heterogeneity between multiple samples in healthy and FGR placentas and to examine potential links between histological changes and the expression of genes involved in placental formation, transport, and transcriptional regulation, and their relationships with fetal growth/pregnancy outcome. Finally, in a proof of principle approach, we integrated these changes into a novel analysis model to better delineate the significance of the placenta in health and disease.

Results:

Patient characteristics

We matched FGR cases and controls for maternal age, booking BMI, mode of delivery and infant sex (Table 1) with expanded clinical data available (Supplementary Table 1). Nonetheless, several significant differences in clinical characteristics were still observed. FGR cases were more likely to be non-White and delivered infants with lower birth and placental weights about a week earlier, although all delivered at term (>36^{+6} weeks of gestation).

Table 1: Patient characteristics.

Characteristics	Control (N=9)	FGR (N=7)	P-value
Maternal age	34.44 ± 1.84	32.00 ± 1.16	0.339
Maternal ethnicity	8 white, 1 non-white	2 white, 5 non-white	0.035
Booking BMI (kg/m^2)	24.67 ± 1.51	24.47 ± 2.75	0.946
Mode of delivery	4 vaginal deliveries, 5 caesarean sections	2 vaginal deliveries, 5 caesarean sections,	0.620
Gestational age at delivery (weeks)	39.14 (39.07 – 39.79)	38.29 (37.29 – 39.00)	0.006
Infant sex	4F, 5M	2F, 5M	0.633
Infant birthweight (kg)	3.53 ± 0.13	2.33 ± 0.18	< 0.001

Placental weight (g)	478.9 ± 16.6	340.7 ± 31.0	0.001

Data are presented as mean ± SEM and were analysed by Student's t test or Mann-Whitney U test. Categorical data were analysed by 2 X 2 contingency table with Fisher's Exact Test. BMI, body mass index; F, female; M, male.

Stereological analysis of placental morphology

Comparing stereological findings by sampling site within the FGR or control groups showed no significant differences between samples taken from the central and peripheral regions of the placenta (Supplementary Table 2). Hence, we averaged the data of the central and peripheral regions of each placenta to compare by pathology (Table 2). Taking into consideration a false discovery rate of 5% for multiple testing, FGR placentas had significantly lower volume densities of intermediate villi, syncytial knots and higher volume densities fibrosis and capillaries. Once placental weight was accounted for, FGR cases showed decreased volumes of intervillous spaces, intermediate villi, terminal villi, syncytial knots, trophoblast and stromal components, and increased volume of fibrosis compared to control placentas. There were no differences in any measure of barrier thickness, surface area, surface densities and diffusion capacities between FGR and control placentas; except that FGR placentas had a decreased villi surface area.

169 **Table 2: Morphological differences in the placenta by pathology**

	Control (N=9)	**FGR (N=7)**	**P-value (^FDR)**
Volume density (cm^3/g)			
Intervillous space	0.37±0.01	0.36±0.02	0.447
Stem villi	0.06±0.01	0.06±0.01	0.895
Intermediate villi	0.12±0.01	0.08±0.01	0.008*
Terminal villi	0.42±0.02	0.4±0.03	0.474
Syncytial knots	0.02±0.00	0.01±0.00	0.002*
Fibrosis	0.01±0.01	0.1±0.02	0.001*
Trophoblast	0.32±0.01	0.34±0.03	0.583
Stromal	0.55±0.02	0.45±0.05	0.058
Capillary	0.13±0.01	0.21±0.03	0.016*
Volume (cm^3)			
Intervillous space	179.73±9.45	119.44±10.77	0.001*
Stem villi	27.83±3.2	20.17±4.25	0.163
Intermediate villi	55.4±4.41	25.48±2.43	<0.001*
Terminal villi	200.73±10.54	135.3±16.23	0.003*
Syncytial knots	8.39±0.78	2.44±0.71	<0.001*
Fibrosis	5.88±3.24	37.02±7.43	0.001*
Trophoblast	153.5±6.83	114.7±13.69	0.017*
Stromal	263.09±15.46	153.23±21.66	0.001*
Capillary	62.3±5.04	72.78±13.76	0.445
Barrier thickness (µm)			
Arithmetic mean	2.83±0.08	2.85±0.18	0.912
Harmonic mean	2.14±0.07	2.24±0.14	0.500
Thickness uniformity index (a measure of thickness variability)	1.32±0.01	1.48±0.08	0.044
Surface density (cm^2/cm^3)			
Villi	610.45±23.85	630.28±44.68	0.683
Fetal capillary	298.26±19.81	401.92±48.29	0.048
Surface area (m^2)			

Villi	11.68±2.88	10.59±1.55	0.009*
Fetal capillary	6.27±1.7	6.89±1.23	0.576
Theoretical diffusion capacity (cm^2/min/kPa)	95.29±4.86	70.26±11.5	0.047
Specific diffusion capacity (cm^2/min/kPa/g)	27.2±1.49	29.47±3.99	0.567

Data presented as mean ± SEM and analysed by t test with FDR (false discovery correction) correction at 5%. * denotes significant findings that passed the 5% FDR.

Placental expression of growth factors and nutrient transporters

We also evaluated relative mRNA expression of selected growth factors and nutrient transporters (Figure 1) that have been previously implicated in transcriptional control or with compromised fetal growth in humans and animal models of FGR[34-39]. Placental *IGF2*, *SLC2A3* and *SLC38A1* expression was significantly lower for FGR versus controls, regardless of sampling location (Figures 1A, 2D and 2E). *VEGFA* expression was significantly lower in the peripheral region as compared to the central region of FGR placentas, while no statistical difference was identified in the central region between cases and controls (Figure 1B). Only *SLC2A1* expression was significantly increased in FGR placenta as compared to controls, independent of sampling location (Figure 1C). No differences in mRNA expression of and *SLC38A2* were observed between FGR and control placentas or by sampling location (Figure 1F). In controls, placental *HNF1A* expression was higher in the peripheral region as compared to the central region (Figure 1G), but no differences were identified for FGR.

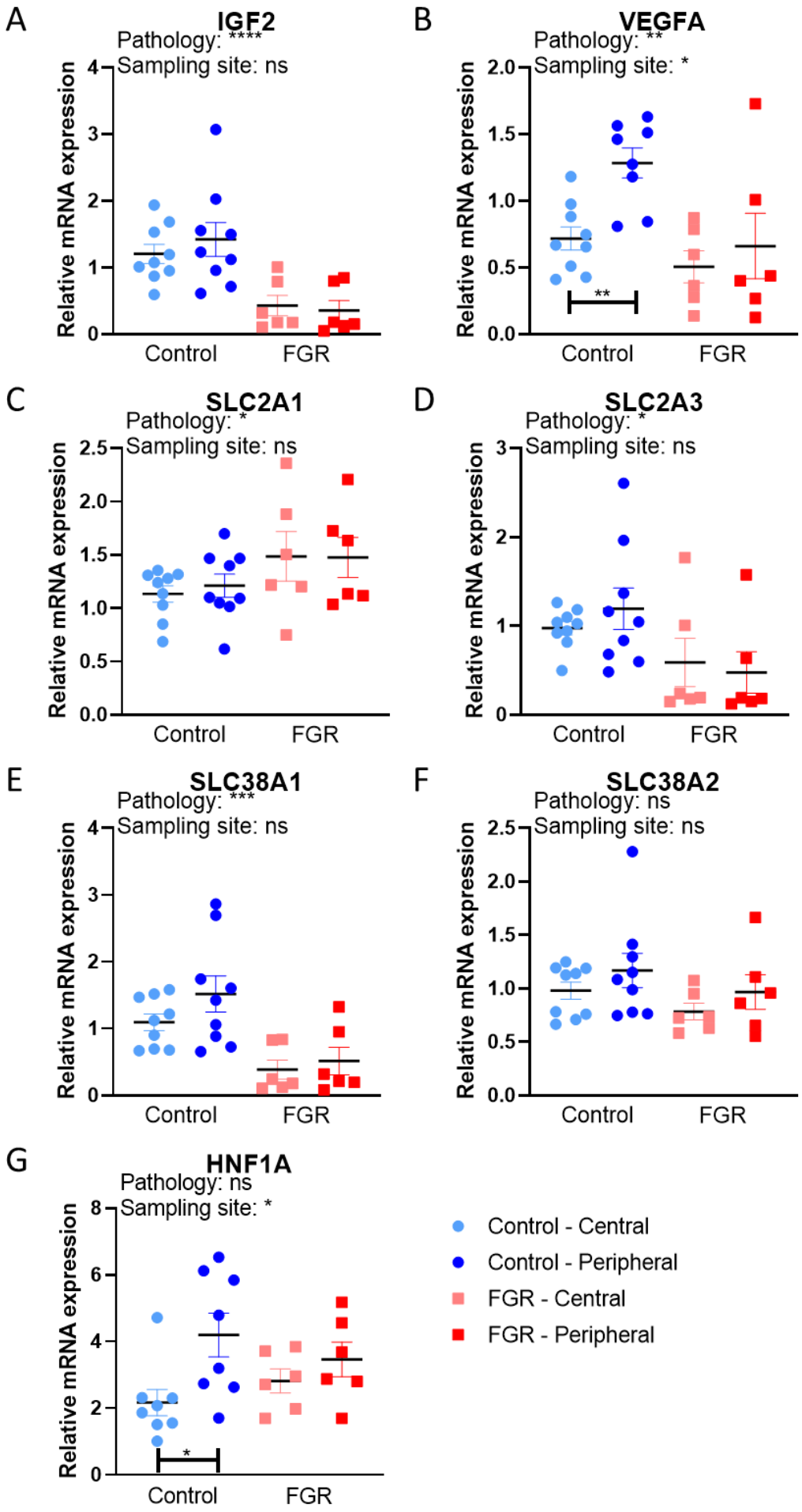

Figure 1: Relative mRNA expression of selected growth factors and nutrient transporters in control and FGR placentas. Expression of growth factors (*IGF2*, *VEGFA*), and transporters (*SLC2A1*, *SLC2A3*, *SLC38A1*, *SLC38A2* and the transcription factor *HNF1A),* were evaluated by qPCR. A total of 3 outliers were excluded; 1 control peripheral value for *VEGFA*, and 1 control central value and 1 control peripheral value for *HNF1A*. Data are presented with individual data points with mean ± SEM and analysed with two-way ANOVA, followed by Sidak's post hoc test for multiple comparisons. *p<0.05, **p<0.01, ***p<0.001, ****p<0.0001.

Associations between placental morphology and expression of functional genes

We next evaluated relationships between placental morphology and the expression of growth factor and nutrient transporter genes within the different sampling sites, and between control and FGR groups using Pearson's r coefficient (Figure 2). In FGR placentas, several inverse correlations were identified between expression of *IGF2, VEGFA, SLC38A1* and *SLC2A3* and the volume of terminal villi, trophoblast, and capillary volume predominantly in the peripheral region of FGR placentas. Inverse correlations with fibrosis volume were also observed for expression *IGF2, VEGFA*, *SLC38A1* and *SLC2A3* in the central region of FGR placentas. Additionally, the relative expression of *IGF2, VEGFA*, *SLC38A1* and *SLC2A3* genes was inversely correlated with barrier thickness uniformity index and both maternal blood spaces and fetal capillaries surface densities in the FGR placenta (central and peripheral sites), although no significant correlations were detected for the control placenta. Moreover, the expression of *IGF2, SLC38A1* and *SLC2A3* genes negatively correlated with both theoretical and specific diffusion capacity in FGR, but not control placentas. In contrast, FGR expression of *HNF1A* showed a positive correlation with specific diffusion capacity in the peripheral region. Positive correlations between the expression of all genes measured and fibrosis and stromal volumes were found for the peripheral region of control placentas, but not FGR placentas. Positive relationships were also seen for expression of *VEGFA* and *HNF1A* with the stem villi volume in central sites of control placentas.

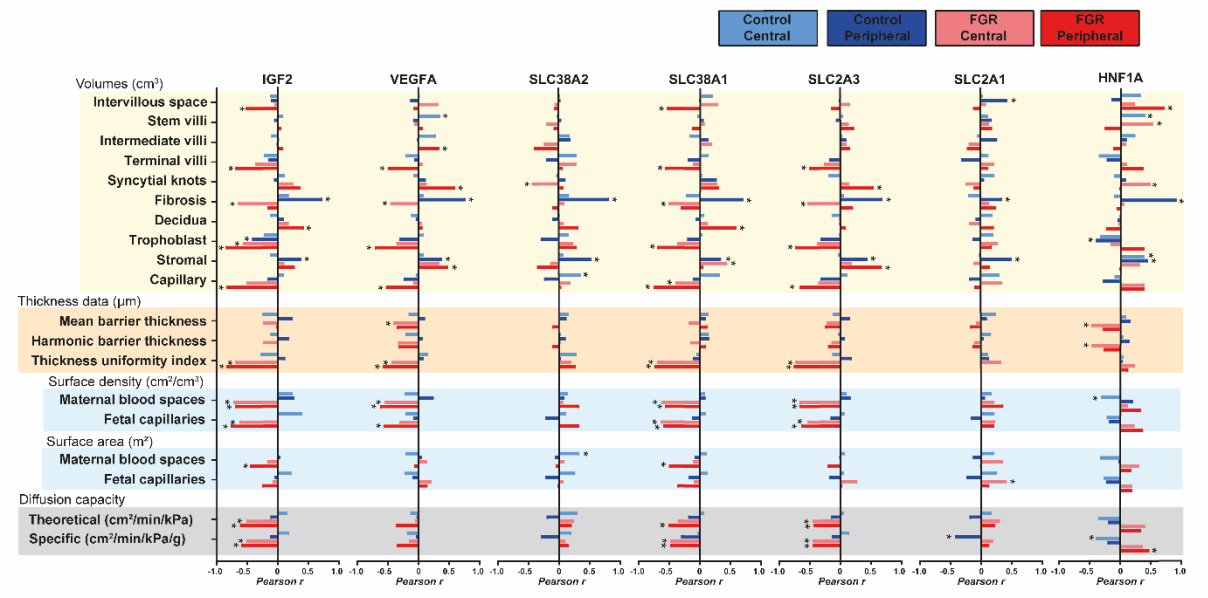

Figure 2. Correlations between stereological parameters and the relative expression of functional genes in the placenta. Pearson's r coefficient was plotted and used to indicate strength of relationship between data (0: low, 1: high) and direction of correlation (+ sign: direct correlation and – sign: inverse correlation). Analysis was performed on each sampling site and experimental group (control and FGR) separately. Sample size was 36 for control and 24 for FGR. *: $p < 0.05$, correlation is statistically significant.

Predictive modelling

To evaluate the information gained from different placental regions/sampling sites (only peripheral, only central, or both together) and data types (only stereological data, only qPCR data or both together), we considered all their possible combinations using predictive modelling (construction of classifiers that would make it possible to distinguish patients in the control group from patients with FGR). As predictive modelling was carried out using three machine learning (ML) methods; *xgbTree*, *glmnet* and *nnet*, this resulted in 27 models for consideration. The binary outcome of FGR was used as an outcome with chosen set of features (only stereological data, only qPCR data, both data types together) used as predictors. The predictive performance of each model was assessed using a leave-one-out cross-validation (LOOCV) scheme: the prediction was made for each patient (with all measurements) by excluding (withholding) it from the dataset, training the classifier on the remaining (independent) samples, and then generating predictions for the withheld samples using the trained model. Using predictions on the training subset (on each round of LOOCV procedures), the best threshold (corresponding to the best sum of sensitivity plus specificity) distinguishing

controls from FGR cases was found and a binary result was calculated for each withheld sample (1 indicated FGR if the prediction was above the threshold, and 0 indicated control if it was below the threshold). Through all rounds, LOOCV procedure binary results were collected for withheld samples and performance was assessed using by these sets of predictions. Performance was estimated using areas under the ROC curve (AUCs) in 2 ways: "AUC for all samples" and "AUC for all patients", as described in Methods. For each combination of "placenta part + type of measurement + ML model" two such AUC values were obtained. Full results of these analyses can be found in Table 3 (in addition, we provide a complete table of errors for each patient in Supplementary Table 3). For a simplified visualization of these results, we considered the distributions of results (AUCs) of different types of ML models on different types of data obtained in different parts of the placenta for all patients and for all their samples separately (Figure 3). This plot clearly shows that among the considered models, the best are those based on measurements performed on the peripheral parts of the placenta and using stereological and qPCR data together. As shown in Table 3, the best model was found to be *nnet*, i.e., the model using simple artificial neural networks for a classification. This model gave the best result for both "AUC for all samples" (0.979) and "AUC for all patients" (0.917). By considering the stereological and qPCR data separately, the stereological data showed a greater predictive power than the qPCR data (Figure 3, for all variants), which, may be due to the clearly different interdependences of the stereological parameters of the control group and the FGR group (the most significant interdependences are presented in Supplementary Figure 1). However, a combination of stereology and qPCR data works better than just stereology for analyses on peripheral parts of the placenta (Figure 3). The results obtained on the central parts of the placenta were lower than the results obtained on both parts of the placenta or only on the peripheral (boxplots for the central parts are slightly lower than the other options). Moreover, results using only peripheral parts were better than using a combination of both parts. Thus, the best model would be that based on measures made on the peripheral parts of the placenta using stereological and qPCR data together.

Table 3: Predictive modelling results using different machine learning methods.

Peripheral & Central									
	Stereology			qPCR			Stereology & qPCR		
	xgbTree	glmnet	nnet	xgbTree	glmnet	nnet	xgbTree	glmnet	nnet
AUC for all samples	0.899	0.913	0.927	0.705	0.733	0.719	0.875	0.92	0.948
AUC for all patients	0.611	0.861	0.917	0.639	0.528	0.528	0.694	0.861	0.917
Peripheral									
	Stereology			qPCR			Stereology & qPCR		
	xgbTree	glmnet	nnet	xgbTree	glmnet	nnet	xgbTree	glmnet	nnet
AUC for all samples	0.903	0.938	0.924	0.681	0.694	0.681	0.819	0.938	**0.979**
AUC for all patients	0.861	0.917	0.861	0.556	0.556	0.556	0.778	0.917	**0.917**
Central									
	Stereology			qPCR			Stereology & qPCR		
	xgbTree	glmnet	nnet	xgbTree	glmnet	nnet	xgbTree	glmnet	nnet
AUC for all samples	0.889	0.903	0.903	0.722	0.694	0.722	0.826	0.889	0.889
AUC for all patients	0.778	0.861	0.861	0.611	0.611	0.611	0.722	0.861	0.806

Results for each combination of "placenta part + type of measurement + ML model" The best version of the model is *nnet* model (highlighted in bold) on peripheral parts of placenta using stereological and qPCR data together. In this case, "AUC for all patients" = 0.917 (corresponding to an error for just one patient-case in a sample of 15 patients: 9 controls and 6 FGR), and "AUC for all samples" = 0.979 (corresponding to an error for only one

measurement, a FGR in a set of 15*4 samples: 9*4 control samples and 6*4 FGR samples). A complete table of errors is given in Supplementary Table 3.

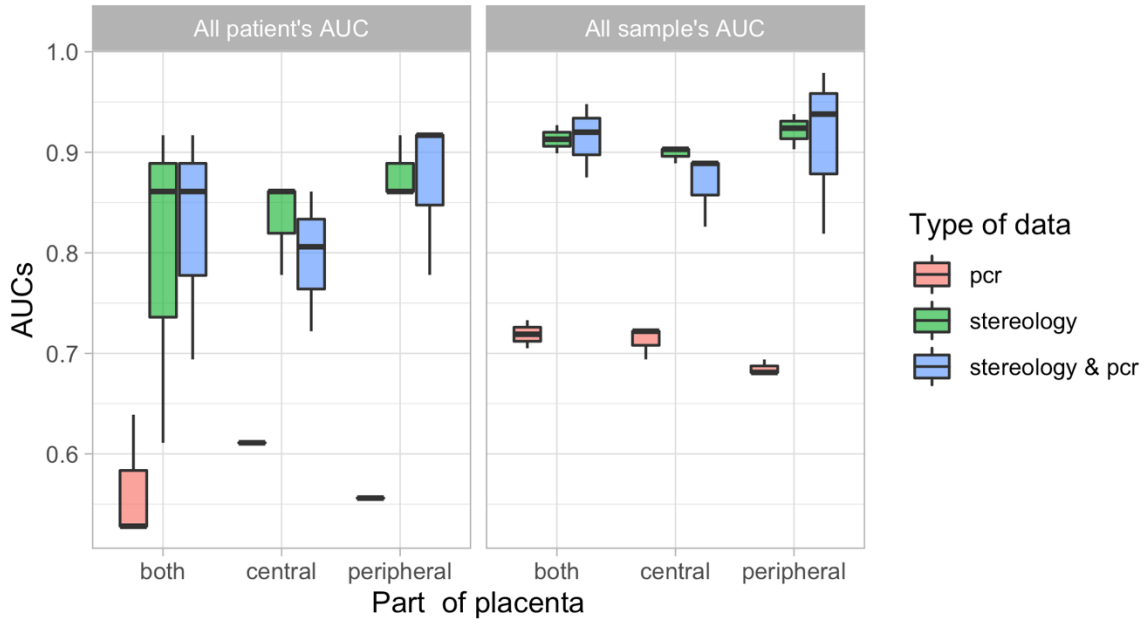

Figure 3: Distributions of AUCs, i.e., the performance results of different types of models on different types of data obtained on different parts of the placenta for all patients and for all their measurements separately.

Discussion

There was no significant variability in the morphological features of the placenta within and between the peripheral and central sites of the placenta, regardless of whether they came from a healthy or FGR pregnancy. In addition, the findings indicate that alterations in placental morphology may be uniform across the placenta in late-onset FGR pregnancies without other complications, such as pre-eclampsia, that can lead to more variable histological changes across the placenta[40].

Despite established evidence that the placenta drives a number of the 'great obstetrical' syndromes, which includes FGR, the relatively poor understanding of underlying placental mechanisms makes interpretation of how they contribute to clinical presentations difficult[41]. Heterogeneity within the placenta is thought to be responsible for some of the difficulties in directly relating disease state to placental findings. Our results suggest that the systematic sampling technique that we used was able to overcome potential morphological spatial heterogeneity of the term placenta, whether from normal or late FGR pregnancies. Indeed,

peripheral versus central region comparisons revealed unique features in gene expression correlations and predictive modelling results. These findings enable more clinical interpretations to be made of the results and indicate that using of this sampling technique may improve reproducibility between placental studies. This analysis suggests that at least a peripheral and central sample should be taken when assessing placental function, particularly in disease states.

Morphological differences between the control and FGR placenta are consistent with findings of others[42], and indicate villous mal-development, with fewer mature intermediate and terminal villi and reduced villous surface area, as well as elevated fibrosis. The increased villous capillary density and reduced syncytial knots in the studied FGR placentas are novel findings and may reflect adaptive responses to hypoxic-reoxygenation events secondary to reduced utero-placental and/or feto-placental flows in FGR pregnancies[43-45]. Moreover, these beneficial changes in placental morphology may be the explanation for the FGR babies in our study reaching near full term. Hence, morphological findings provide a clue to underlying placental mechanisms that may be subject to change, with the resultant amelioration of disease and improvement to fetal outcome, if they can be enacted *in utero*. There is already significant interest in delivery of targeted agents to the uterine arteries to improve blood flow[46]. Delivery of agents to target specific areas of pathology and functional deficit within the placenta to improve the clinical condition may also be a potential therapeutic option.

Our approach to combine morphological assessments with gene expression aimed to identify some key aetiological pathways for the pathology seen. Expression of placental *IGF2*, *SLC2A3* and *SLC38A1* was lower across the FGR placenta, correlating with volumes and other specific placental features, suggesting a global role for these molecules in placental structure and development in the presence of FGR. Indeed, *IGF2* is known to be important for the formation of the placental exchange interface in humans, among other species[38,39,47], and is expressed at lower levels in placentas showing FGR/small for gestational age in some[48,49], but not all studies[50]. Prior work has shown that a genetic deficiency of *SLC2A3* in mice leads to FGR [37] which supports our findings, but is in contrast to other work reporting an upregulation of its encoded protein in the human placenta of late-onset FGR[51]. Of the system A amino acid transporters expressed by the human placenta, *SLC38A1* is key for system A activity at term[52]. Other work has also shown that placental system A activity is reduced in explants prepared from term FGR placentas[53]. *VEGFA* was significantly lower in the peripheral region of the

placenta in FGR and correlated to the following placental pathology (terminal villi, trophoblast and capillary volume) that might suggest a causal association. This is consistent with other work reporting lower placental *VEGFA* expression at term in late onset FGR[54,55], and the involvement of angiogenic factors more generally in normal and pathological pregnancies[56]. Our findings also have relevance for emerging pre-clinical research in placenta-directed gene therapy for FGR, including the utility of insulin-like growth factors and angiogenic regulators[57]. *HNF1A* was more highly expressed by the peripheral region compared with central region in healthy, but not FGR placentas. Little is known about the function of *HNF1A* in the placenta, although the human tissue atlas[58] indicates it is abundantly expressed by the villous syncytiotrophoblast [59]. Recent work has highlighted that *HNF1A* may regulate a large number of genes in trophoblast cells[60] and mediate metabolic changes[61], which could be important for the placental support of fetal growth, more broadly.

Using a modelling approach in our discovery cohort, we demonstrated the potential of predicting outcome (control or FGR) based on stereology and qPCR data. Stereology and qPCR measurements taken from the peripheral part of the placenta, and analysed together, have the highest predictive power. To avoid any possible overfitting of the models, we did not perform any feature selection in advance for tuning of the algorithm hyperparameters. Despite this, we were able to obtain predictions with very high accuracy, as, in fact, for the best model, only one sample out of 60 (4 samples from peripheral placenta part for each of 15 patients) considered was predicted incorrectly. Indeed, this subject was one that was most likely to be misclassified in all of the tested models. Nevertheless, we found that the morphological data clearly shows separation of features for control and FGR placentas and probably, this made it possible to obtain high quality constructed models. For the present study, we used a very strict LOOCV. Whilst modelling predictions were poor when qPCR data were used alone, adding these data to the analysis of stereology data improved prediction, hence, confirming importance of qPCR data and underlying link of these data with functional features. Whilst our modelling approach shows potential, future work would benefit from utilising a larger dataset, with extremes of pathology, to validate the model.

Overall, our data add to current understanding of placental function through comprehensive sampling of healthy placentas and those affected by disease (FGR) with careful deep histological analysis, integrated with expression of genes involved in key biological pathways regulating placental function. Whilst, our modelling approach requires validation, with further

pathology analysed, it offers the promise of better diagnostic yield and novel insight into biological pathways that affect FGR pregnancies.

Material and methods:

Placental tissue collection and sampling

Subjects were recruited from University College London Hospital NHS Foundation Trust, London, UK with ethics approval from the South-Central Oxford A research ethics committee (17/SC/0432). After written informed consent was obtained, term placental biopsies were collected from subjects diagnosed with late-onset FGR (n=7, FGR detected after 32 weeks' gestation and an estimated fetal weight and/or abdominal circumference below 3rd centile on population-based charts used clinically[62]), and from control subjects with appropriately grown fetuses (n=9 birthweight >10th centile and <90th centile). Data on maternal pre-existing conditions, previous obstetric history, ultrasound examination, and pregnancy complications were collected at the time of recruitment.

Placentas were weighed and sampled within 30 minutes of delivery. Sampling sites were chosen to be representative of four central and four peripheral regions always relative to cord insertion (Figure 4A). In marginal cord insertions, the placenta was orientated with the cord anterior. Sampling then took place relative to the cord insertion as in other cases. This meant there was one site that had less tissue to sample from initially, in non-central cord insertions, but that ultimately the same amount of tissue was sampled, and that tissue selection was directly related to the cord in the same way as all other samples. For each placenta, 8 tissue biopsies (with maternal tissue and fetal chorionic plate removed) were snap frozen using liquid nitrogen or dry ice and stored at -80°C. Neighboring sampling sites were then immersion-fixed in 4% paraformaldehyde.

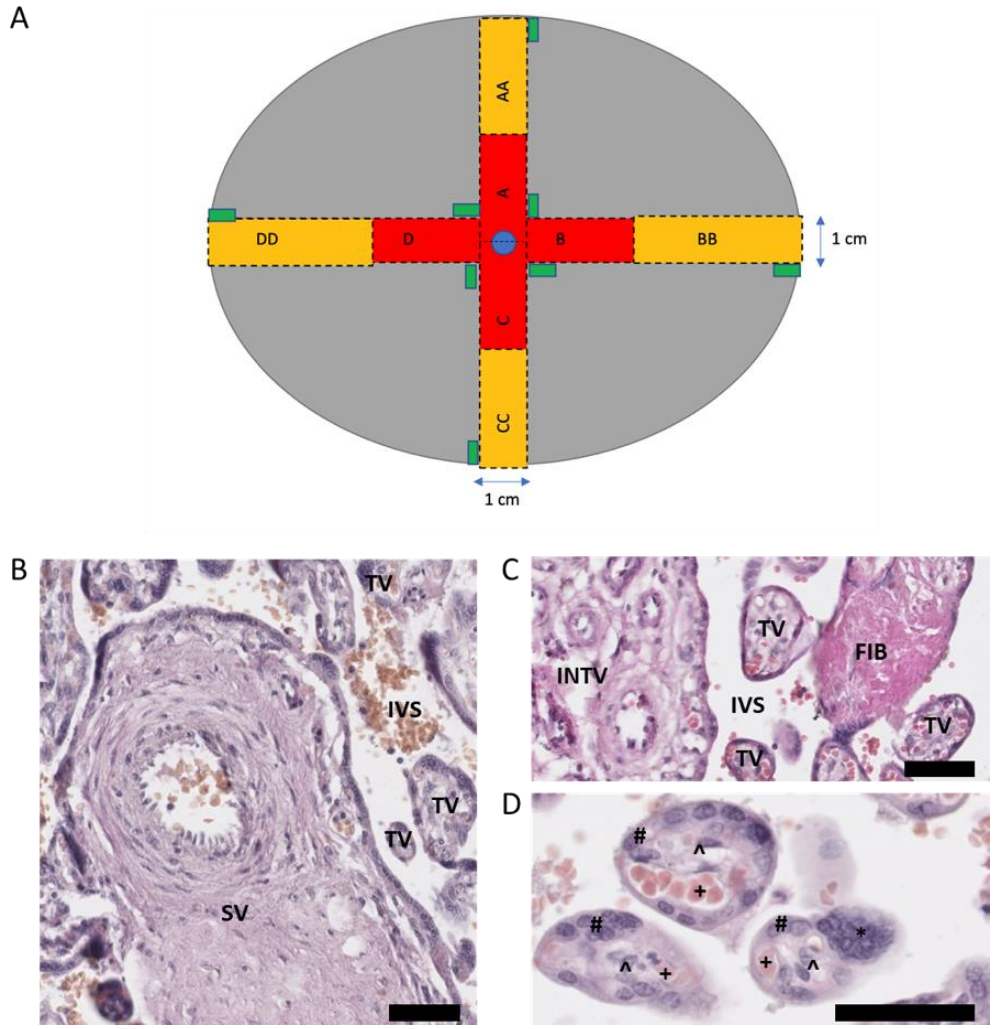

Figure 4. Diagram showing sampling of placenta (A) and main parameters measured in histological sections of placenta (B-D). (**A**) Dotted lines indicate where the placenta should be cut with a sterile histology knife. Red boxes with single letters indicate inner sections. Yellow boxes with double letters indicate outer sections. Green rectangles represent samples taken for RNA sampling. The central blue circle represents the umbilical cord (cut). (**B-D**) Representative histological sections of term human placenta. Stereological analysis was performed by identifying the intervillous space (IVS), stem villi (SV), intermediate villi (INTV), terminal villi (TV), fibrosis (FIB), syncytial knots (*); and under higher magnification of terminal villi, the trophoblast cell layer (#), fetal capillaries (+) and stromal cells (^). The scale bar denotes 50µm.

406 ***RNA extraction, cDNA synthesis and qPCR***

407 Total RNA was extracted from n=9 control and n=6 FGR frozen placental tissues (n=1 FGR
408 sample was not taken due to >30 minute delay in freezing this sample) using the RNeasy
409 Fibrous Tissue Mini Kit (Qiagen, Hilden, Germany) following the manufacturer's protocol.
410 Briefly, approximately 2mg of tissue was added to 300µl of lysis buffer and homogenized
411 using a bead-based technique. Following treatment with proteinase K and addition of 100%
412 ethanol, the homogenate was transferred to the spin columns, washed with supplied buffers
413 and centrifuged to remove contaminants. Purified RNA was then eluted into RNase-free water.
414 Quality and concentration of extracted RNA were determined by Nanodop (Thermo Fisher
415 Scientific, Waltham, CA, USA).
416
417 Complementary DNA (cDNA) was synthesized using the Applied Biosystems High-Capacity
418 cDNA Reverse Transcription Kit (Thermo Fisher Scientific) according to manufacturer's
419 instructions on a thermal cycler. Real-time PCR was performed in duplicate using TaqMan™
420 Universal Master Mix II, with UNG (Thermo Fisher Scientific) and inventoried TaqMan®
421 gene expression assay probes with either VIC and FAM fluorophores for 5 housekeeping genes
422 (*18SrRNA*, *B2M*, *GAPDH*, *GUSB* and *YWHAZ*) and 8 genes of interest (*HNF1A*, *IGF2*,
423 *SLC2A1*, *SLC2A3*, *SLC38A1*, *SLC38A2*, *SLC38A4* and *VEGFA*) (Table 4). Only stable
424 housekeeping genes (*18S rRNA*, *B2M*, *GADPH* and *YWHAZ*) that showed no statistically
425 significant differences between cases and controls were included in the housekeeper geomean
426 calculation for normalising gene expression across samples. The relative expression of genes
427 of interest was then calculated using the $2^{-\Delta\Delta Ct}$ method.
428
429 **Table 4 Probes used for real-time PCR**

Analysed genes	Gene symbol	Probe ID	Fluorophore
Housekeeping genes	*18S rRNA*	Hs99999901_s1	VIC
	B2M	Hs00187842_m1	VIC
	GAPDH	Hs02786624_g1	VIC
	GUSB	Hs00939627_m1	VIC
	YWHAZ	Hs01122445_g1	VIC
Genes of interest	*HNF1A*	Hs00167041_m1	VIC
	IGF2	Hs04188276_m1	FAM
	SLC2A1	Hs00892681_m1	FAM

	SLC2A3	Hs00359840_m1	FAM
	SLC38A1	Hs01562175_m1	FAM
	SLC38A2	Hs01089954_m1	VIC
	SLC38A4	Hs00394339_m1	FAM
	VEGFA	Hs00900055_m1	FAM

Histological preparation

Following paraformaldehyde fixation, biopsies of 8 sites from each control (n=9) and FGR (n=7) placenta were embedded in paraffin using routine histological techniques and sectioned at 7µm thickness. Sections were rehydrated using xylene and ethanol gradients, stained with haematoxylin and eosin, dehydrated with ethanol gradients and xylene, then mounted with DPX. Slides were then scanned using a Nanozoomer digital slide scanner (Hamamatsu Photonics, Shizuoka Prefecture, Japan).

Placental stereology

Placentas were analysed blinded to the diagnosis of FGR. To perform stereological analysis in a manner similar to that performed previously[63]; transparent lattices with test points, test lines or test arcs were superimposed onto scanned images viewed under different magnification on the NDP.view2 software (Hamamatsu Photonics). Volume densities of the intervillous space, stem villi, intermediate villi, terminal villi, syncytial knots, and fibrosis (Figure 4B-C) were estimated by point counting and a lattice of equally spaced test points arranged 4 by 4 under 10X magnification in at least 13 fields of view for a minimum of 200 measurements per section. Volume densities of the trophoblast, stroma, and fetal capillaries (Figure 4D) within villi were estimated under a similar lattice under 40X magnification in 20 fields of view per sample. Absolute placental volumes were estimated by multiplying volume densities with placental weight (g). Arithmetic barrier thickness was assessed under 100X magnification in 20 fields of view per sample and a superimposed lattice with equally spaced straight test lines, which at times, intersected fetal capillary and villous trophoblast involved in exchange. The ‘measure’ tool within the software was then used to determine the shortest distance between a fetal capillary and the maternal blood space, where there was an intersection. Mean harmonic barrier thickness was calculated using the inverse of mean reciprocal of each raw arithmetic barrier thickness measurement. Thickness uniformity index, as a measure of the variability in thickness across the villous membrane, was obtained from the ratio of the mean arithmetic

458 barrier thickness to the mean harmonic barrier thickness. Surface densities were approximated
459 by counting chance intersections of fetal capillaries and villous trophoblast involved in
460 exchange with superimposed test arc lines under 40X magnification. To derive surface areas,
461 surface densities were multiplied by placental villous volume. The theoretical diffusion
462 capacity was calculated using the total surface area for exchange (averaged surface area of fetal
463 capillaries and villi) divided by the mean harmonic barrier thickness and multiplied by Krogh's
464 constant for oxygen diffusion. Specific diffusion capacity was then calculated by dividing the
465 theoretical diffusion capacity by the infant birthweight.
466
467 ***Predictive modelling***
468 To evaluate the informativity of different placental sampling locations (only peripheral, only
469 central or both regions together) and different data types (only stereological data, only PCR
470 data or both types together), we studied all their possible combinations with analysis performed
471 in R (version 4.0.2). To analyse several well-established multi-dimensional methods of data
472 analysis, the machine learning models (*xgbTree*, *glmnet* and *nnet*) were implemented using
473 *caret* package (version 6.0.90). All 27 models were trained with default set of hyperparameters,
474 cross-validated on 5 folds (for a better selection of internal algorithm parameters), with seed
475 parameter set to 123. The performance of models was assessed with receiver operating
476 characteristic (ROC) curves using area under the curve (AUC) with 95% confidence intervals
477 (*pROC* package, version 1.18.0). Results of AUCs were presented in two ways:
478 - *All sample's AUC* - Calculating AUC considering all samples as independent;
479 - *All patient's AUC* - Calculating AUC on patient's result's only (if all samples belonging
480 to one patient were correctly predicted, then we assumed that a prediction for this
481 patient was correct, if the prediction was wrong in at least one sample of the sample's
482 patient, then it was set as wrong for this patient).
483 For illustration of interdependencies of features, which are presented in Supplementary Figure
484 1, we selected the best pairs that showed significant differences between FGR and control
485 groups using ANOVA test after applying FDR (false discovery rate) adjustment to test's p-
486 values (*stats* package, Version 4.0.2).
487
488 ***Statistical analyses***
489 Normality of data was assessed by D'Agostino-Pearson normality test. ROUT testing for
490 outliers was used to identify any outliers, which were then excluded from the analysis. For
491 comparisons between 2 groups, Student's t tests and Mann-Whitney U tests were performed

for parametric and non-parametric continuous data, respectively. Categorical data between FGR and controls were analysed by a 2 X 2 contingency table with Fisher's Exact Test. Two-way ANOVAs followed by Sidak post hoc test for multiple comparisons were used to analyse mRNA expression data by pathology and sampling location. Graphpad Prism 6.01 (Graphpad Software Inc., La Jolla, CA, USA) was used for statistical analyses. A p-value of <0.05 was considered statistically significant for clinical characteristics and mRNA expression analysis. To account for multiple testing in histological analyses, a false discovery rate correction at 5% was applied to determine statistical significance.

Acknowledgements

ANSP received funding for this work via an Academy of Medical Sciences Springboard Grant, Dorothy Hodgkin Research Fellowship (DH130036/RG74249), MRC New Investigator Grant (MR/R022690/1/RG93186) and Lister Institute of Preventative Medicine Research Prize (RG93692). TN and AZ are supported by a Medical Research Council grant (MR/R02524X/1). HEJY was supported by an A*STAR International Fellowship from the Agency for Science, Technology and Research. KM was supported by UCLH Charity and the Mitchell Charitable Trust. SLH received funding for this work via an Academy of Medical Sciences Clinical Lecturer Starter Grant and the UCLH EGA Obstetric Charity.

Author contributions

HEJY, KM, SLH and ANSP designed the study. HEJY, KM, MABY, ESP collected and/or performed experiments. HEJY, KM, ESP and TN analysed and graphed the data. TN and AZ provided predictive modelling analysis. HEJY, KM, TN, AZ, ALD, SLH and ANSP interpreted the data. HEJY, KM, SLH and ANSP wrote the paper. All authors performed final editing checks and approved the final manuscript.

519 **References**

520

521 1 Napso, T., Yong, H. E., Lopez-Tello, J. & Sferruzzi-Perri, A. N. The role of placental
522 hormones in mediating maternal adaptations to support pregnancy and lactation.
523 *Front Physiology* **9:1091**, doi:10.3389/fphys.2018.01091 (2018).
524 2 Burton, G. J., Fowden, A. L. & Thornburg, K. L. Placental Origins of Chronic Disease.
525 *Physiological reviews* **96**, 1509-1565, doi:10.1152/physrev.00029.2015 (2016).
526 3 Byrne, M. *et al.* Structure-function relationships in the feto-placental circulation
527 from in silico interpretation of micro-CT vascular structures. *J Theor Biol* **517**,
528 110630, doi:10.1016/j.jtbi.2021.110630 (2021).
529 4 Aughwane, R. *et al.* Micro-CT and histological investigation of the spatial pattern of
530 feto-placental vascular density. *Placenta* **88**, 36-43,
531 doi:10.1016/j.placenta.2019.09.014 (2019).
532 5 World Health, O. *Every newborn: an action plan to end preventable deaths*. 55 p.
533 (World Health Organization, 2014).
534 6 Lawn, J. E. *et al.* Every Newborn: progress, priorities, and potential beyond survival.
535 *Lancet* **384**, 189-205, doi:10.1016/S0140-6736(14)60496-7 (2014).
536 7 Sharma, D., Shastri, S. & Sharma, P. Intrauterine Growth Restriction: Antenatal and
537 Postnatal Aspects. *Clin Med Insights Pediatr* **10**, 67-83, doi:10.4137/CMPed.S40070
538 (2016).
539 8 Gordijn, S. J. *et al.* Consensus definition of fetal growth restriction: a Delphi
540 procedure. *Ultrasound Obstet Gynecol* **48**, 333-339, doi:10.1002/uog.15884 (2016).
541 9 Van den Berg, B. J. & Yerushalmy, J. The relationship of the rate of intrauterine
542 growth of infants of low birth weight to mortality, morbidity, and congenital
543 anomalies. *J Pediatr* **69**, 531-545, doi:10.1016/s0022-3476(66)80038-0 (1966).
544 10 Bianchi, M. E. & Restrepo, J. M. Low Birthweight as a Risk Factor for Non-
545 communicable Diseases in Adults. *Front Med (Lausanne)* **8**, 793990,
546 doi:10.3389/fmed.2021.793990 (2021).
547 11 Caradeux, J., Martinez-Portilla, R. J., Basuki, T. R., Kiserud, T. & Figueras, F. Risk of
548 fetal death in growth-restricted fetuses with umbilical and/or ductus venosus absent
549 or reversed end-diastolic velocities before 34 weeks of gestation: a systematic
550 review and meta-analysis. *Am J Obstet Gynecol* **218**, S774-S782 e721,
551 doi:10.1016/j.ajog.2017.11.566 (2018).
552 12 Ishihara, N. *et al.* Increased apoptosis in the syncytiotrophoblast in human term
553 placentas complicated by either preeclampsia or intrauterine growth retardation.
554 *Am J Obstet Gynecol* **186**, 158-166, doi:10.1067/mob.2002.119176 (2002).
555 13 Mayhew, T. M., Wijesekara, J., Baker, P. N. & Ong, S. S. Morphometric evidence that
556 villous development and fetoplacental angiogenesis are compromised by
557 intrauterine growth restriction but not by pre-eclampsia. *Placenta* **25**, 829-833,
558 doi:10.1016/j.placenta.2004.04.011 (2004).
559 14 Macara, L. *et al.* Structural analysis of placental terminal villi from growth-restricted
560 pregnancies with abnormal umbilical artery Doppler waveforms. *Placenta* **17**, 37-48,
561 doi:10.1016/s0143-4004(05)80642-3 (1996).
562 15 Teasdale, F. & Jean-Jacques, G. Intrauterine growth retardation: morphometry of the
563 microvillous membrane of the human placenta. *Placenta* **9**, 47-55 (1988).

16 Burton, G. J. & Fowden, A. L. The placenta: a multifaceted, transient organ. *Philos Trans R Soc Lond B Biol Sci* **370**, 20140066, doi:10.1098/rstb.2014.0066 (2015).
17 Chavatte-Palmer, P. & Tarrade, A. Placentation in different mammalian species. *Ann Endocrinol (Paris)* **77**, 67-74, doi:10.1016/j.ando.2016.04.006 (2016).
18 Pere, M. C. Materno-foetal exchanges and utilisation of nutrients by the foetus: comparison between species. *Reprod Nutr Dev* **43**, 1-15, doi:10.1051/rnd:2003002 (2003).
19 Crawford, M. A., Hassam, A. G. & Williams, G. Essential fatty acids and fetal brain growth. *Lancet* **1**, 452-453, doi:10.1016/s0140-6736(76)91476-8 (1976).
20 Gresham, E. L., Simons, P. S. & Battaglia, F. C. Maternal-fetal urea concentration difference in man: metabolic significance. *J Pediatr* **79**, 809-811, doi:10.1016/s0022-3476(71)80396-7 (1971).
21 Sferruzzi-Perri, A. N. *et al.* Placental-specific Igf2 deficiency alters developmental adaptations to undernutrition in mice. *Endocrinology* **152**, 3202-3212, doi:10.1210/en.2011-0240 (2011).
22 Sferruzzi-Perri, A. N. *et al.* An obesogenic diet during mouse pregnancy modifies maternal nutrient partitioning and the fetal growth trajectory. *Faseb J* **27**, 3928-3937, doi:10.1096/fj.13-234823 (2013).
23 Vaughan, O. R., Sferruzzi-Perri, A. N. & Fowden, A. L. Maternal corticosterone regulates nutrient allocation to fetal growth in mice. *The Journal of physiology* **590**, 5529-5540 (2012).
24 Higgins, J. S., Vaughan, O. R., de Liger, E. F., Fowden, A. L. & Sferruzzi-Perri, A. N. Placental phenotype and resource allocation to fetal growth are modified by the timing and degree of hypoxia during mouse pregnancy. *J Physiol* **594**, 1341-1356, doi:10.1113/JP271057 (2015).
25 Napso, T., Hung, Y. P., Davidge, S. T., Care, A. S. & Sferruzzi-Perri, A. N. Advanced maternal age compromises fetal growth and induces sex-specific changes in placental phenotype in rats. *Sci Rep* **9**, 16916, doi:10.1038/s41598-019-53199-x (2019).
26 Lewis, R. M. & Sferruzzi-Perri, A. N. in *Developmental Origins of Health and Disease* (eds L. Poston, K. M. Godfrey, M. A. Hanson, & P. Gluckman) (Cambridge University Press).
27 Audette, M. C., McLaughlin, K. & Kingdom, J. C. Second Trimester Placental Growth Factor Levels and Placental Histopathology in Low-Risk Nulliparous Pregnancies. *J Obstet Gynaecol Can* **43**, 1145-1152 e1141, doi:10.1016/j.jogc.2021.01.018 (2021).
28 Burton, G. J. *et al.* Optimising sample collection for placental research. *Placenta* **35**, 9-22, doi:10.1016/j.placenta.2013.11.005 (2014).
29 Mayhew, T. M. Taking tissue samples from the placenta: an illustration of principles and strategies. *Placenta* **29**, 1-14, doi:10.1016/j.placenta.2007.05.010 (2008).
30 Mayhew, T. M. Morphomics: An integral part of systems biology of the human placenta. *Placenta* **36**, 329-340, doi:10.1016/j.placenta.2015.01.001 (2015).
31 Salafia, C. M. *et al.* Placental surface shape, function, and effects of maternal and fetal vascular pathology. *Placenta* **31**, 958-962, doi:10.1016/j.placenta.2010.09.005 (2010).
32 Gordon, Z. *et al.* Anthropometry of fetal vasculature in the chorionic plate. *J Anat* **211**, 698-706, doi:10.1111/j.1469-7580.2007.00819.x (2007).

33 Heifetz, S. A. The umbilical cord: obstetrically important lesions. *Clin Obstet Gynecol* **39**, 571-587, doi:10.1097/00003081-199609000-00007 (1996).
34 Sferruzzi-Perri, A. N. & Camm, E. J. The programming power of the placenta. *Frontiers in Physiology* **7:33**, doi:10.3389/fphys.2016.00033 (2016).
35 Vaughan, O. R. *et al.* Placenta-specific Slc38a2/SNAT2 knockdown causes fetal growth restriction in mice. *Clin Sci (Lond)* **135**, 2049-2066, doi:10.1042/CS20210575 (2021).
36 Luscher, B. P. *et al.* Placental glucose transporter (GLUT)-1 is down-regulated in preeclampsia. *Placenta* **55**, 94-99, doi:10.1016/j.placenta.2017.04.023 (2017).
37 Ganguly, A. *et al.* Glucose transporter isoform-3 mutations cause early pregnancy loss and fetal growth restriction. *American journal of physiology* **292**, E1241-1255 (2007).
38 Sferruzzi-Perri, A. N., Owens, J. A., Pringle, K. G. & Roberts, C. T. The neglected role of insulin-like growth factors in the maternal circulation regulating fetal growth. *The Journal of physiology* **589**, 7-20 (2010).
39 Sferruzzi-Perri, A. N., Sandovici, I., Constancia, M. & Fowden, A. L. Placental phenotype and the insulin-like growth factors: resource allocation to fetal growth. *The Journal of physiology* **595**, 5057-5093 (2017).
40 Mifsud, W. & Sebire, N. J. Placental pathology in early-onset and late-onset fetal growth restriction. *Fetal Diagn Ther* **36**, 117-128, doi:10.1159/000359969 (2014).
41 Brosens, I., Pijnenborg, R., Vercruysse, L. & Romero, R. The "Great Obstetrical Syndromes" are associated with disorders of deep placentation. *Am J Obstet Gynecol* **204**, 193-201, doi:10.1016/j.ajog.2010.08.009 (2011).
42 Burton, G. J. & Jauniaux, E. Pathophysiology of placental-derived fetal growth restriction. *Am J Obstet Gynecol* **218**, S745-S761, doi:10.1016/j.ajog.2017.11.577 (2018).
43 Kovo, M. *et al.* Placental vascular lesion differences in pregnancy-induced hypertension and normotensive fetal growth restriction. *Am J Obstet Gynecol* **202**, 561 e561-565, doi:10.1016/j.ajog.2010.01.012 (2010).
44 Colson, A., Sonveaux, P., Debieve, F. & Sferruzzi-Perri, A. N. Adaptations of the human placenta to hypoxia: opportunities for interventions in fetal growth restriction. *Hum Reprod Update*, doi:10.1093/humupd/dmaa053 (2020).
45 Cindrova-Davies, T. & Sferruzzi-Perri, A. N. Human placental development and function. *Seminars in Cell and Developmental Biology* **In press** (2022).
46 David, A. L. *et al.* Local delivery of VEGF adenovirus to the uterine artery increases vasorelaxation and uterine blood flow in the pregnant sheep. *Gene Ther* **15**, 1344-1350, doi:10.1038/gt.2008.102 (2008).
47 Sferruzzi-Perri, A. N. Regulating needs: Exploring the role of insulin-like growth factor-2 signalling in materno-fetal resource allocation. *Placenta* **Suppl 1**, S16-S22, doi:10.1016/j.placenta.2018.01.005 (2018).
48 Guo, L. *et al.* Altered gene expression and methylation of the human chromosome 11 imprinted region in small for gestational age (SGA) placentae. *Dev Biol* **320**, 79-91, doi:10.1016/j.ydbio.2008.04.025 (2008).
49 Yamaguchi, Y. *et al.* Placenta-specific epimutation at H19-DMR among common pregnancy complications: its frequency and effect on the expression patterns of H19 and IGF2. *Clin Epigenetics* **11**, 113, doi:10.1186/s13148-019-0712-3 (2019).

50 Antonazzo, P. *et al.* Placental IGF2 Expression in Normal and Intrauterine Growth Restricted (IUGR) Pregnancies. *Placenta* **29**, 99-101 (2008).
51 Janzen, C. *et al.* Placental glucose transporter 3 (GLUT3) is up-regulated in human pregnancies complicated by late-onset intrauterine growth restriction. *Placenta* **34**, 1072-1078, doi:10.1016/j.placenta.2013.08.010 (2013).
52 Desforges, M., Greenwood, S. L., Glazier, J. D., Westwood, M. & Sibley, C. P. The contribution of SNAT1 to system A amino acid transporter activity in human placental trophoblast. *Biochem Biophys Res Commun* **398**, 130-134, doi:10.1016/j.bbrc.2010.06.051 (2010).
53 Shibata, E. *et al.* Placental System A Amino Acid Transport is Reduced in Pregnancies With Small For Gestational Age (SGA) Infants but Not in Preeclampsia with SGA Infants. *Placenta* **29**, 879-882 (2008).
54 Lash, G. *et al.* Abnormal fetal growth is not associated with altered chorionic villous expression of vascular endothelial growth factor mRNA. *Mol Hum Reprod* **7**, 1093-1098, doi:10.1093/molehr/7.11.1093 (2001).
55 Lyall, F., Young, A., Boswell, F., Kingdom, J. C. & Greer, I. A. Placental expression of vascular endothelial growth factor in placentae from pregnancies complicated by pre-eclampsia and intrauterine growth restriction does not support placental hypoxia at delivery. *Placenta* **18**, 269-276, doi:10.1016/s0143-4004(97)80061-6 (1997).
56 Andraweera, P. H., Dekker, G. A. & Roberts, C. T. The vascular endothelial growth factor family in adverse pregnancy outcomes. *Hum Reprod Update* **18**, 436-457, doi:10.1093/humupd/dms011 (2012).
57 Krishnan, T. & David, A. L. Placenta-directed gene therapy for fetal growth restriction. *Semin Fetal Neonatal Med* **22**, 415-422, doi:10.1016/j.siny.2017.04.005 (2017).
58 Uhlen, M. *et al.* Proteomics. Tissue-based map of the human proteome. *Science* **347**, 1260419, doi:10.1126/science.1260419 (2015).
59 Human Protein Atlas Team. *Human Protein Atlas - HNF1A in the placenta*, <https://www.proteinatlas.org/ENSG00000135100-HNF1A/tissue/placenta> (
60 Ducat, A. *et al.* Low-dose aspirin protective effects are correlated with deregulation of HNF factor expression in the preeclamptic placentas from mice and humans. *Cell Death Discov* **5**, 94, doi:10.1038/s41420-019-0170-x (2019).
61 Rout, M. & Lulu, S. S. Molecular and disease association of gestational diabetes mellitus affected mother and placental datasets reveal a strong link between insulin growth factor (IGF) genes in amino acid transport pathway: A network biology approach. *J Cell Biochem*, doi:10.1002/jcb.27418 (2018).
62 Brenner, W. E., Edelman, D. A. & Hendricks, C. H. A standard of fetal growth for the United States of America. *Am J Obstet Gynecol* **126**, 555-564, doi:10.1016/0002-9378(76)90748-1 (1976).
63 Mayhew, T. M. Stereology and the placenta: where's the point? -- a review. *Placenta* **27 Suppl A**, S17-25, doi:10.1016/j.placenta.2005.11.006 (2006).

SUPPLEMENTARY INFORMATION

Supplementary Table 1: Full phenotype clinical data.

ID	Status	Medical history	Pregnancy complications	Maternal age quartile (years)	Ethnicity	Maternal booking BMI	Delivery mode	Gestation	Birthweight (g)	Infant sex	Placenta weight (g)	Placenta/ BW ratio (%)	Analysis comments
Control 1	Control			31-35	Asian	34	Vaginal delivery	39+6	3200	Male	442	13.8	
Control 2	Control			36-40	White	21	cat4 CS	39+1	3690	Female	516	14.0	
Control 3	Control			21-25	White	20	Vaginal delivery	39+0	3800	Female	534	14.1	
Control 4	Control			31-35	White	23	cat3 CS	41+1	3970	Male	509	12.8	
Control 5	Control			41-45	White	27	cat4 CS	39+1	3960	Female	481	12.1	
Control 6	Control			36-40	White	24	cat4 CS	39+1	2893	Female	413	14.3	
Control 7	Control			36-40	White	23	Vaginal delivery	39+0	3618	Male	491	13.6	
Control 8	Control			36-40	White	23	cat4 CS	39+1	3140	Male	398	12.7	
Control 9	Control			31-35	White	28	Vaginal delivery	39+5	3510	Male	526	15.0	
FGR 1	Late FGR			31-35	White	23	cat3 CS	37+0	1410	Male	160	11.3	

FGR 2	Late FGR	Hypothyroid		31-35	White	22	Vaginal delivery	37+5	2510	Female	346	13.8	
FGR 3	Late FGR	Migraines		31-35	Chinese	22	cat2 CS	37+2	2560	Male	380	14.8	
FGR 4	Late FGR		Low platelets	26-30	Afro Caribbean	22	cat2 CS	38+2	1985	Male	380	19.1	
FGR 5	Late FGR			31-35	Chinese	20	Vaginal delivery	39+4	2720	Female	360	13.2	
FGR 6	Late FGR		Gestational diabetes	31-35	Asian	38	cat1 CS	38+4	2396	Male	355	14.8	
FGR 7	Late FGR			36-40	Afro Caribbean	28	cat3 CS	39+0	2750	Male	404	14.7	Not run for qPCR

CS = caesarean section. Cat1 = Immediate threat to the life of the woman or fetus, Cat2 = Maternal or fetal compromise which is not immediately life-threatening, Cat3 = No maternal or fetal compromise but needs early birth, Cat4 = Birth timed to suit woman or healthcare provider. (NICE guideline 192: Caesarean birth, published 31 March 2021).

Supplementary Table 2: Morphological differences in the placenta by sampling location.

	Control (N=9)			**FGR (N=7)**		
	Central	**Peripheral**	**P-value**	**Central**	**Peripheral**	**P-value**
Volume density (cm^3/g)						
Intervillous space	0.39±0.02	0.36±0.01	0.130	0.36±0.02	0.35±0.02	0.577
Stem villi	0.06±0.01	0.06±0.01	0.902	0.06±0.02	0.05±0.01	0.364
Intermediate villi	0.1±0.01	0.13±0.01	0.105	0.08±0.01	0.08±0.01	0.720
Terminal villi	0.42±0.02	0.42±0.02	0.941	0.41±0.03	0.38±0.03	0.526
Syncytial knots	0.02±0.00	0.02±0.00	0.633	0.01±0.00	0.01±0.00	0.591
Fibrosis	0.01±0.00	0.02±0.01	0.443	0.07±0.02	0.13±0.03	0.091
Trophoblast	0.33±0.02	0.31±0.01	0.492	0.34±0.02	0.33±0.04	0.818
Stromal	0.53±0.03	0.57±0.02	0.239	0.45±0.04	0.46±0.06	0.865
Capillary	0.14±0.01	0.12±0.01	0.139	0.21±0.03	0.21±0.03	0.963
Volume (cm^3)						
Intervillous space	187.75±10.19	171.7±9.96	0.277	121.96±11.52	116.92±10.14	0.748
Stem villi	27.82±5.18	27.85±2.89	0.100	23.24±6.3	17.1±2.58	0.385
Intermediate villi	49.91±4.81	60.89±5.94	0.170	24.77±2.83	26.19±2.23	0.700
Terminal villi	199.23±8.7	202.24±13.7	0.855	141.08±17.48	129.51±15.51	0.630
Syncytial knots	8.89±0.9	7.89±1.12	0.495	2.24±0.66	2.63±0.82	0.720
Fibrosis	3.9±1.93	7.87±4.69	0.446	26.28±6.89	47.77±9.57	0.094
Trophoblast	156.49±6.76	150.51±8.25	0.583	117.28±13.22	112.13±15.07	0.802

Stromal	254.68±18.75	271.49±12.97	0.472	150.39±19.02	156.07±25.00	0.860
Capillary	67.72±5.88	56.89±5.04	0.181	73.05±14.18	72.51±13.58	0.979
Barrier thickness (μm)						
Arithmetic mean	2.84±0.08	2.82±0.10	0.885	2.84±0.19	2.86±0.18	0.940
Harmonic mean	2.14±0.07	2.15±0.07	0.918	2.24±0.15	2.24±0.14	0.987
Thickness uniformity index	1.33±0.02	1.31±0.02	0.508	1.47±0.08	1.48±0.08	0.936
Surface density (cm^2/cm^3)						
Villi	613.67±27.94	607.22±24.07	0.863	634.49±43.19	626.07±47.42	0.898
Fetal capillary	318.63±27.71	277.88±13.62	0.206	406.06±47.11	397.78±51.52	0.906
Surface area (m^2)						
Villi	15.32±0.97	15.99±0.92	0.622	10.87±1.63	10.3±1.51	0.801
Fetal capillary	7.89±0.75	7.32±0.44	0.519	7.11±1.31	6.67±1.2	0.807
Theoretical diffusion capacity (cm^2/min/kPa)	94.95±5.96	95.64±4.31	0.926	71.63±11.95	68.89±11.61	0.872
Specific diffusion capacity (cm^2/min/kPa/g)	27.15±1.86	27.24±1.23	0.968	30.24±4.58	28.7±3.71	0.798

Supplementary Table 3: Summary tables of errors in all 27 models for each patient.

ONLY PERIPHERAL										
id	score	STEREOLOGY & PCR			PCR			STEREOLOGY		
		xgbTree	glmnet	nnet	xgbTree	glmnet	nnet	xgbTree	glmnet	nnet
Control 1	0	0of4	0of4	0of4	1of4	1of4	1of4	0of4	0of4	0of4
Control 2	0	1of4	0of4	0of4	0of4	0of4	0of4	1of4	0of4	0of4
Control 3	0	0of4	0of4	0of4	0of4	1of4	1of4	0of4	0of4	0of4
Control 4	0	0of4	0of4	0of4	4of4	3of4	3of4	0of4	0of4	0of4
Control 5	0	0of4	0of4	0of4	2of4	0of4	0of4	0of4	0of4	0of4
Control 6	0	0of4	0of4	0of4	3of4	3of4	4of4	0of4	0of4	0of4
Control 7	0	0of4	0of4	0of4	0of4	0of4	0of4	0of4	0of4	0of4
Control 8	0	0of4	0of4	0of4	1of4	2of4	2of4	0of4	0of4	1of4
Control 9	0	0of4	0of4	0of4	0of4	0of4	0of4	0of4	0of4	0of4
FGR 1	1	4of4	0of4	0of4	4of4	4of4	4of4	0of4	0of4	0of4
FGR 2	1	0of4	0of4	0of4	0of4	0of4	0of4	0of4	0of4	0of4
FGR 3	1	0of4	0of4	0of4	0of4	0of4	0of4	0of4	0of4	0of4
FGR 4	1	0of4	0of4	0of4	0of4	0of4	0of4	0of4	0of4	0of4
FGR 5	1	0of4	0of4	0of4	0of4	0of4	0of4	0of4	0of4	0of4
FGR 6	1	4of4	3of4	1of4	4of4	4of4	4of4	4of4	3of4	3of4

ONLY CENTRAL										
id	score	STEREOLOGY & PCR			PCR			STEREOLOGY		
		xgbTree	glmnet	nnet	xgbTree	glmnet	nnet	xgbTree	glmnet	nnet
Control 1	0	0of4	0of4	0of4	0of4	0of4	0of4	0of4	0of4	0of4
Control 2	0	0of4	0of4	0of4	0of4	0of4	0of4	0of4	0of4	0of4
Control 3	0	0of4	0of4	0of4	2of4	2of4	0of4	0of4	0of4	0of4
Control 4	0	0of4	0of4	0of4	2of4	3of4	3of4	0of4	0of4	0of4
Control 5	0	0of4	0of4	0of4	0of4	0of4	0of4	0of4	0of4	0of4
Control 6	0	3of4	2of4	1of4	3of4	3of4	3of4	0of4	0of4	0of4
Control 7	0	0of4	0of4	0of4	0of4	0of4	0of4	0of4	0of4	0of4
Control 8	0	2of4	0of4	1of4	0of4	0of4	1of4	2of4	1of4	1of4
Control 9	0	0of4	0of4	0of4	1of4	2of4	1of4	0of4	0of4	0of4
FGR 1	1	1of4	0of4	0of4	4of4	4of4	4of4	0of4	0of4	0of4
FGR 2	1	0of4	0of4	0of4	0of4	0of4	0of4	0of4	0of4	0of4
FGR 3	1	0of4	0of4	0of4	0of4	0of4	0of4	0of4	0of4	0of4
FGR 4	1	0of4	0of4	0of4	0of4	0of4	0of4	1of4	0of4	0of4
FGR 5	1	0of4	0of4	0of4	0of4	0of4	0of4	0of4	0of4	0of4
FGR 6	1	4of4	4of4	4of4	4of4	4of4	4of4	3of4	4of4	4of4

CENTRAL & PERIPHERAL										
id	score	STEREOLOGY & PCR			PCR			STEREOLOGY		
		xgbTree	glmnet	nnet	xgbTree	glmnet	nnet	xgbTree	glmnet	nnet
Control 1	0	1of8	0of8	0of8	1of8	1of8	1of8	1of8	0of8	0of8
Control 2	0	0of8	0of8	0of8	0of8	0of8	0of8	0of8	0of8	0of8
Control 3	0	0of8	0of8	0of8	1of8	2of8	2of8	0of8	0of8	0of8
Control 4	0	0of8	0of8	0of8	5of8	2of8	5of8	0of8	0of8	0of8
Control 5	0	0of8	0of8	0of8	2of8	0of8	0of8	0of8	0of8	0of8
Control 6	0	3of8	1of8	0of8	6of8	7of8	6of8	0of8	0of8	0of8
Control 7	0	0of8	0of8	0of8	0of8	0of8	0of8	1of8	0of8	0of8
Control 8	0	1of8	0of8	0of8	1of8	1of8	1of8	1of8	2of8	0of8
Control 9	0	1of8	0of8	0of8	1of8	0of8	0of8	1of8	0of8	0of8
FGR 1	1	0of8	0of8	0of8	8of8	8of8	8of8	0of8	0of8	0of8
FGR 2	1	0of8	0of8	0of8	0of8	0of8	0of8	0of8	0of8	0of8
FGR 3	1	0of8	0of8	0of8	1of8	0of8	0of8	1of8	0of8	0of8
FGR 4	1	0of8	0of8	0of8	0of8	0of8	0of8	0of8	0of8	0of8
FGR 5	1	0of8	0of8	0of8	0of8	1of8	1of8	0of8	0of8	0of8
FGR 6	1	8of8	7of8	5of8	8of8	8of8	8of8	6of8	7of8	7of8

Each cell for each patient and 27 models considered (different columns) indicates how many wrong predictions were made for this patient among all 4 or 8 available samples (for example, the entry 0of4 means that 0 errors were made among 4 predictions). The cell is highlighted in

red if at least one mistake was made for the patient. Third column in the first panel corresponds to the best model, using *nnet* ML algorithm, and both stereology and PCR data for peripheral samples. This model returns only one wrong prediction out of 60 samples considered.

Supplementary Figure 1: Different interdependencies of features for stereological data.

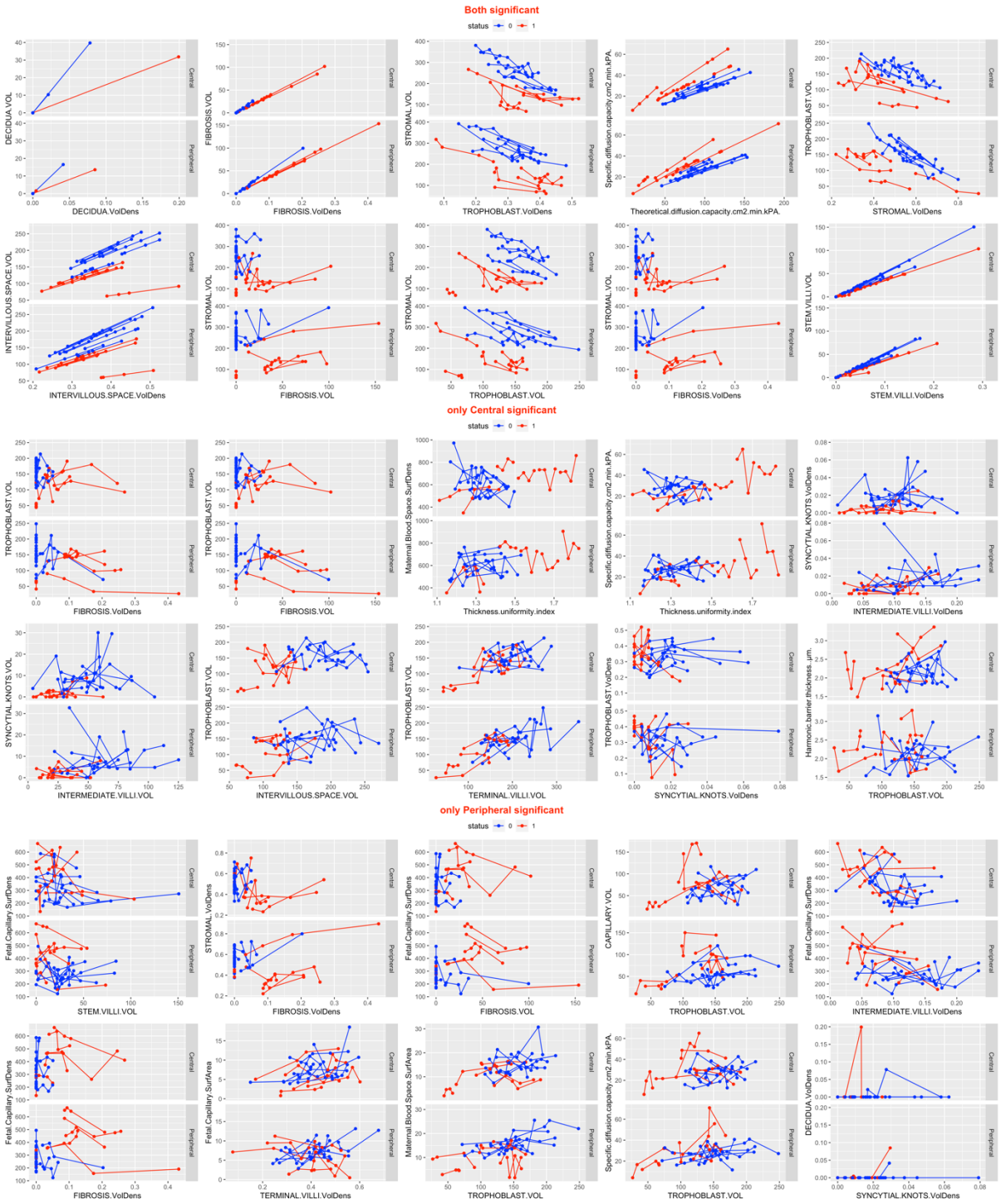

Different interdependencies of features for Control (blue colour) and FGR (red colour) on stereological data. Each point is a separate patient measurement, each line connects all measurements for each patient. For many pairs of features, a separation between FGR cases and controls was easily seen, hence, enabling a construction of a successful predictive model.